

Scaling and modeling of heat-release effects on subfilter turbulence in premixed combustion

By J. F. MacArt[†] AND M. E. Mueller[‡]

Conventional large-eddy simulation (LES) subfilter turbulence closures are compared with heat-release-enabled models in low- and high-Karlovitz-number turbulent premixed jet flames. Direct numerical simulation (DNS) databases are filtered with a Gaussian kernel, and the resulting subfilter statistics are compared with *a priori* model predictions. The conventional closures perform well at high Karlovitz number, despite local heat-release effects, while models that account for small-scale expansion are necessary at low Karlovitz number. These models are then implemented in *a posteriori* LES calculations, and only the physical heat-release closure is found to correctly account for subfilter flame-induced turbulence production.

1. Introduction

Interactions between turbulence and combustion heat release can dramatically alter turbulence dynamics in certain regimes of turbulent premixed combustion, potentially invalidating conventional subfilter turbulence model assumptions. When a flame is thin relative to turbulence scales, combustion-induced pressure dilatation becomes a significant source of turbulent kinetic energy (TKE) and is balanced by negative production; that is, the mean shear production term becomes a sink of TKE (Cheng 1984). Negative production is associated with the phenomenon of countergradient transport (CGT) (Moss 1980; Bray *et al.* 1981) and inverse-cascade energy transfer from the small scales of turbulence to large scales (O'Brien *et al.* 2014, 2017). These effects can invalidate conventional dissipative turbulence models based on Boussinesq/Smagorinsky or gradient-diffusion assumptions (Veynante *et al.* 1997; MacArt *et al.* 2018).

Scaling arguments (Bilger 2004) for turbulent premixed combustion suggest that energy transfer by pressure-dilatation mechanisms becomes the dominant source of TKE when the flame timescale is fast compared with the timescales of viscous dissipation. This timescale dependence may be recast in terms of the local Karlovitz number $Ka \equiv t_F/t_\eta$ and a critical Karlovitz number $Ka_{cr} \equiv \tau$, where $t_F \equiv \delta_F/s_L$ is the laminar flame timescale, $t_\eta \equiv (\nu/\epsilon)^{1/2}$ is the Kolmogorov timescale, and $\tau \equiv \rho_u/\rho_b - 1$ is the flame density ratio. In the preceding expressions, δ_F is the laminar flame thickness, s_L is the laminar flame speed, ν is the kinematic viscosity, ϵ is the TKE dissipation rate, and ρ_u and ρ_b are the densities of the unburned and burned gas, respectively. Effects of combustion-induced dilatation on the turbulence, including inverse-cascade transfer and CGT, should be apparent when $Ka \ll Ka_{cr}$. In the opposite extreme, when $Ka \gg Ka_{cr}$, large-scale turbulent straining balances viscous dissipation as in nonreacting turbulence, and pressure dilatation plays a negligible role (MacArt *et al.* 2018).

The turbulence modeling requirements in these two limit states are well understood. At

[†] Center for Exascale Simulation of Plasma-Coupled Combustion, University of Illinois at Urbana-Champaign

[‡] Department of Mechanical and Aerospace Engineering, Princeton University

low Karlovitz number ($Ka \ll Ka_{cr}$), turbulence essentially undergoes rapid distortion by the flame (O'Brien *et al.* 2017), leading to widespread inverse-cascade transfer (O'Brien *et al.* 2014; Towery *et al.* 2016). The resulting CGT may be modeled with algebraic closures (Veynante *et al.* 1997; MacArt *et al.* 2018), in which countergradient terms obtained from infinitely thin flame theory (Bray *et al.* 1981) are linearly combined with gradient-type turbulence models with blending functions to control the relative weight of the two. Since heat-release effects in this rapid-distortion regime will never be resolved in large-eddy simulation (LES), the modeling requirements are the same as those for the Reynolds-averaged Navier-Stokes (RANS) approach; in particular, algebraic closures should be equally suitable for LES at any resolution as the are for RANS. Conversely, at high Karlovitz number ($Ka \gg Ka_{cr}$), the flame scales are large relative to the turbulence scales, and heat release does not significantly disrupt the balance between production and dissipation (Hamlington *et al.* 2011). In the limit of infinite Karlovitz number and for sufficiently high Reynolds number, the turbulence is essentially unmodified by heat release, and nonreacting turbulence models remain valid.

Between these two limit states, an intermediate regime exists in which heat release occurring more slowly than viscous dissipation ($Ka \gtrsim Ka_{cr}$) can result in an active cascade (O'Brien *et al.* 2017) in which competition exists between the inverse cascade associated with heat release and the classical forward cascade (Towery *et al.* 2016). Turbulence modeling requirements in this regime depend on the relative magnitude of these two competing processes at the filter scale. The relative dominance of one process over the other is hypothesized to be parameterized by the filter Damköhler number, $Da_\Delta \equiv t_\Delta/t_F$, where $t_\Delta \equiv (\Delta^2/\epsilon)^{1/3}$ is the timescale of turbulence with a characteristic size equal to the LES filter width Δ . At large Da_Δ (relatively fast heat release and/or slow filter-scale turbulence), significant subfilter heat-release effects may be expected; conversely, at small Da_Δ (relatively slow heat release and/or fast filter-scale turbulence), subfilter heat-release effects should be negligible. Stated equivalently, in the active-cascade regime, as the filter width decreases, Da_Δ decreases, and the effects of heat release on subfilter turbulence are expected to diminish. The focus of the current study is on the low- and high-Karlovitz number regimes; challenges with accessing the intermediate regime are discussed at the end of Section 4.

This report summarizes analyses of effects of the heat release on subfilter turbulence in the low- and high-Karlovitz number regimes of turbulent premixed combustion. Direct numerical simulation (DNS) databases and analogous LES calculations are described in Section 2. The performance of three turbulence models is evaluated *a priori* by filtering the DNS databases and *a posteriori* by implementation into analogous LES calculations. These turbulence models are described and results are reported for a single filter width in Section 3. The scaling of the subfilter scalar flux and the model performance are discussed as a function of the filter width in Section 4. Conclusions, including the need for databases in the active-cascade regime, are drawn in Section 5.

2. Computational implementation

Three-dimensional DNS and LES of turbulent premixed planar jet flames are performed. The flames develop in the streamwise (x) and cross-stream (y) directions and are statistically homogeneous in the spanwise (z) direction. An unburned hydrogen-air mixture at stoichiometric ($\phi = 1.0$) equivalence ratio enters the domain through a central jet at bulk Reynolds number $Re_0 \equiv U_0 H_0 / \nu = 5,000$, where U_0 is the jet bulk velocity

and H_0 is the jet height. This mixture is diluted 20 % by volume with nitrogen to avoid flashback at low central jet velocities. The central jet is separated from symmetric laminar coflow jets by thin walls. Equilibrium products of the same hydrogen-air premixture enter the domain through the coflow jets, ensuring flame stability at high central-jet velocities. The critical Karlovitz number of this mixture is $Ka_{cr} = 6.7$.

Two configurations are simulated at in-flame Karlovitz numbers $Ka_{\hat{C}=0.5} = 3.7$ (denoted 5P-K1) and $Ka_{\hat{C}=0.5} = 54.0$ (denoted 5P-K2), which correspond to integral-scale Damköhler numbers $Da = 0.6$ and $Da = 0.05$, respectively. In-flame properties are evaluated at mean reaction progress variable $\hat{C} = 0.5$, where the reaction progress variable C is defined as the normalized molecular oxygen mass fraction. Mean quantities, denoted $\hat{\phi}$, are obtained at instants in time by averaging over the statistically homogeneous spanwise (z) direction.

In the DNS calculations, the density ρ , velocity u_i , pressure p , temperature T , and reacting species mass fractions Y_k are obtained in the low-Mach-number limit by solving the coupled Navier-Stokes equations, enthalpy equation, and reacting species equations in conservative form. In the LES calculations, equations for the equivalent Favre-filtered quantities are solved with models for the subfilter stress in the momentum equation and the subfilter scalar flux in the scalar equations. Models are also applied to close the filtered chemical source terms in the scalar equations. The subfilter stress is defined as $\tau_{ij}^r = \widetilde{u_i u_j} - \widetilde{u}_i \widetilde{u}_j$, and the subfilter scalar flux is defined as $F_{j,k} = \widetilde{u_j Y_k} - \widetilde{u}_j \widetilde{Y}_k$. Further details on the configuration and DNS databases may be found in MacArt *et al.* (2018). The *a posteriori* LES calculations of these flames are described in Section 3.4.

3. Subfilter turbulence model evaluation

Models for the subfilter scalar flux and stress are described in Sections 3.1 and 3.2, respectively. Results of the *a priori* and *a posteriori* analyses are presented in Sections 3.3 and 3.4, respectively.

3.1. Subfilter scalar flux models

Three subfilter scalar flux models are evaluated and compared. The first is the constant-coefficient Smagorinsky-like model for the scalar flux

$$F_{j,k}^{\text{Smag}} = -\frac{(c_s \Delta)^2}{Sc_t} \tilde{S} \frac{\partial \tilde{Y}_k}{\partial x_j}, \quad (3.1)$$

where $c_s = 0.12$ is the Smagorinsky constant, $Sc_t = 0.65$ is a turbulent Schmidt number, and $\tilde{S} = (2\tilde{S}_{ij}\tilde{S}_{ij})^{1/2}$ is the magnitude of the filtered strain-rate tensor. The turbulent Schmidt number was chosen by fitting the modeled RANS scalar flux to DNS-evaluated statistics in case 5P-K2 (MacArt *et al.* 2018).

The second model follows the form of algebraic RANS closures (Veynante *et al.* 1997; MacArt *et al.* 2018). A countergradient term obtained in the infinitely-thin-flame (zero-Karlovitz-number) limit (Bray *et al.* 1981) is linearly superposed with Eq. (3.1), which is generally valid only in the infinite-Karlovitz-number limit. The resulting model, denoted the linear algebraic heat release (LAHR) model, is written in the LES context as

$$F_{j,k}^{\text{LAHR}} = F_{j,k}^{\text{Smag}} + \alpha \frac{(\tilde{Y}_k - \tilde{Y}_{k,u})(\tilde{Y}_{k,b} - \tilde{Y}_k)}{\tilde{Y}_{k,b} - \tilde{Y}_{k,u}} \tau_{SL} n_j, \quad (3.2)$$

where α is an efficiency function that controls the relative weight of the two terms and

n_j is the j -th component of the flame-normal vector. A functional form of the efficiency function that contains a weak Da_Δ dependence is obtained

$$\alpha = c_\alpha \left(\frac{s_L \delta_F}{\nu} \right)^{-1/2} Da_\Delta^{1/2}, \quad (3.3)$$

where the model constant is set to $c_\alpha = 1.4$ as in previous work. Further details on the model formulation may be found in MacArt *et al.* (2018).

Finally, the method of Clark *et al.* (1979) using a Taylor series expansion gives rise to a model of the form

$$F_{j,k}^{\text{Clark}} = \frac{\Delta_i^2}{12} \frac{\partial \tilde{u}_j}{\partial x_i} \frac{\partial \tilde{Y}_k}{\partial x_i}, \quad (3.4)$$

where Δ_i is the local filter width in the i -th direction, and the factor of 12 originates from the Taylor series expansion assuming a Gaussian filter kernel. The local characteristic filter width is obtained from the product of the local directional filter widths: $\Delta = (\Pi_i \Delta_i)^{1/3}$.

3.2. Subfilter stress models

The subfilter stress models considered here are analogous to the subfilter scalar flux models described above, and therefore only a brief overview of the former is given. The constant-coefficient Smagorinsky model for the deviatoric subfilter (residual) stress is

$$\tau_{ij}^{r,\text{Smag}} = -2(c_s \Delta)^2 \tilde{S} \left(\tilde{S}_{ij} - \frac{1}{3} \tilde{S}_{kk} \delta_{ij} \right), \quad (3.5)$$

where the constant is $c_s = 0.12$ as before and δ_{ij} is the Kronecker delta function. The algebraic modifications in the zero-Karlovitz-number limit result in the LAHR model,

$$\tau_{ij}^{r,\text{LAHR}} = \tau_{ij}^{r,\text{Smag}} + \alpha^2 \tilde{C} (1 - \tilde{C}) (\tau s_L)^2 \left(n_i n_j - \frac{1}{3} \delta_{ij} \right), \quad (3.6)$$

where α is obtained from Eq. (3.3) as before with $c_\alpha = 1.4$. Finally, the model of Clark *et al.* (1979) is written as

$$\tau_{ij}^{r,\text{Clark}} = \frac{\Delta_k^2}{12} \frac{\partial \tilde{u}_i}{\partial x_k} \frac{\partial \tilde{u}_j}{\partial x_k}. \quad (3.7)$$

3.3. *A priori* analysis

The relative performance of the subfilter turbulence models is now compared in an *a priori* sense. The DNS databases are filtered with an inhomogeneous Gaussian filter kernel obtained as the product of one-dimensional filter kernels with $\Delta_i = 16\delta_i$, where δ_i is the nonuniform DNS grid spacing. The inhomogeneous filter width is representative of realistic LES calculations in the nonreacting flow regions, and thermal expansion results in a filter width of approximately five times the in-flame Kolmogorov scale ($\Delta \approx 5\eta_{\hat{C}=0.5}$). The effective resolution corresponds to approximately one to four LES grid cells per δ_F in both flames. The effects of increasing the filter width are discussed in Section 4. The turbulence models presented in Sections 3.1 and 3.2 are evaluated with the filtered statistics obtained from the DNS, and the resulting subfilter predictions are compared with the small-scale DNS statistics. Since the mean flame-normal vector is aligned mainly with the cross-stream direction, in which the affects of heat release are most apparent, an analysis of the cross-stream statistics is also provided below.

Figure 1 shows the cross-stream component of the subfilter H₂O mass fraction flux

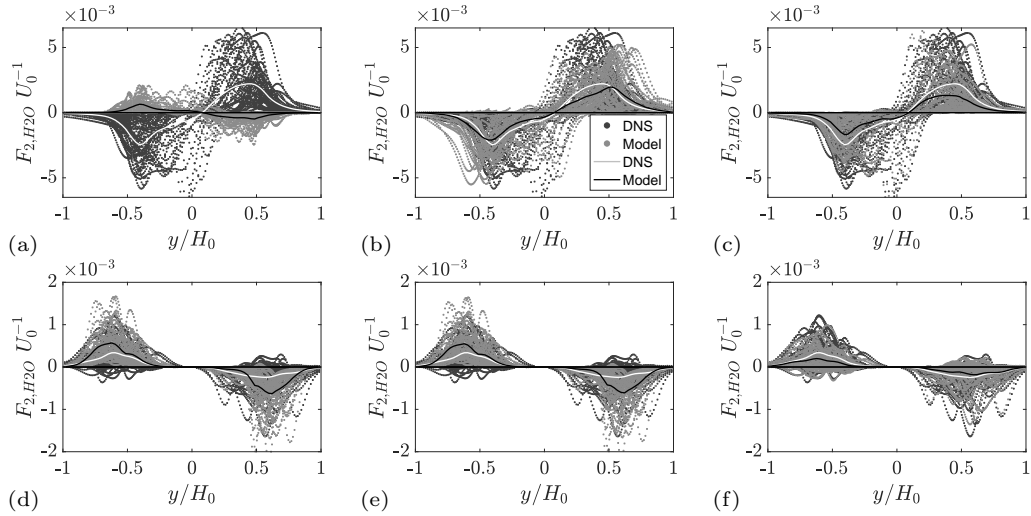


FIGURE 1. Comparison of DNS-evaluated cross-stream subfilter scalar flux and *a priori* model predictions. Instantaneous y - z scatter data are shown as points; instantaneous spatial (z) means are shown as solid lines. Top row: 5P-K1, bottom row: 5P-K2. (a,d) Smagorinsky model, (b,e) LAHR model, (c,f) Clark model.

evaluated from DNS and the three models. Instantaneous statistics are shown at the streamwise location $x/H_0 = 3$ for all cross-stream and spanwise locations, and the corresponding spanwise averages are shown as solid lines.

In 5P-K1, the cross-stream subfilter scalar flux is entirely countergradient, as evidenced by positive DNS statistics for $y/H_0 > 0$ and vice versa. The Smagorinsky model incorrectly captures the sign of the scalar flux [Figure 1(a)], predicting gradient transport rather than CGT. When the countergradient term is superposed in the LAHR model, the model captures CGT and is in visual agreement with the DNS. The Clark model also captures the CGT in 5P-K1 but consistently underpredicts the magnitude.

In 5P-K2, the scalar flux satisfies the gradient-transport hypothesis in the mean. Nonetheless, smaller, locally reversed fluxes are observed instantaneously. The Smagorinsky model qualitatively captures the gradient behavior [Figure 1(d)] but does not capture any of the local CGT. The countergradient term in the LAHR model is effectively inactive at the lower filter Damköhler number, resulting in predictions that are nearly identical to those of the Smagorinsky model. The Clark model succeeds in capturing some of the local sign reversal but again underpredicts the DNS-evaluated fluxes, and the extent of this underprediction increases with increasing filter width (discussed further in Section 4).

Figure 2 shows the subfilter shear stress evaluated from DNS and the three models described in Section 3.2. The shear component (τ_{12}^r) was observed to be affected most significantly by low-Karlovitz-number heat release in analogous RANS-type analysis (MacArt *et al.* 2018) and is therefore considered here.

In 5P-K1, instantaneous counter-Boussinesq transport is observed and is not captured by the Smagorinsky model [Figure 2(a)]. The heat-release term in the LAHR model is inactive [Figure 2(b)] despite the availability of the instantaneous flame-normal vector (unlike the analogous RANS model). This counter-Boussinesq transport is likely due to pressure-strain redistribution (MacArt *et al.* 2018), for which more complex subfilter closures are necessary. Conversely, the Clark model performs remarkably well at low

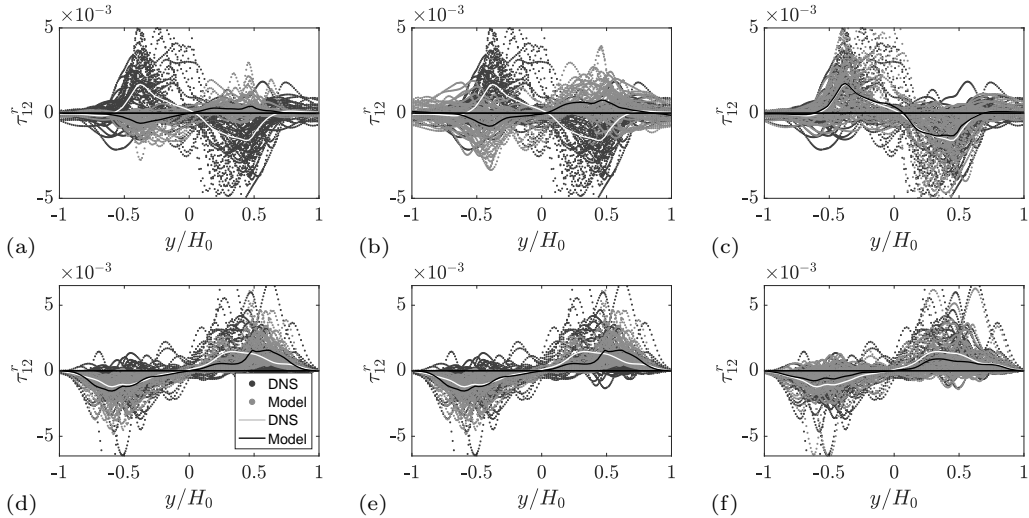


FIGURE 2. Comparison of DNS-evaluated subfilter shear stress and *a priori* model predictions. Instantaneous y - z scatter data are shown as points; instantaneous spatial (z) means are shown as solid lines. Top row: 5P-K1, bottom row: 5P-K2. (a,d) Smagorinsky model, (b,e) LAHR model, (c,f) Clark model.

Karlovitz number and appears to be the model of choice. These results contrast with the model performance in 5P-K2, in which the Clark model underpredicts the magnitude of the subfilter stress.

3.4. *A-posteriori* analysis

A-posteriori LES calculations were computed with the same code as the DNS databases using the three sets of subfilter transport models described above. The LES grid is coarsened by a factor of approximately eight in each direction, so the total number of grid points is decreased by a factor of approximately 500 compared with the DNS calculations. LES calculations with grids coarsened by factors of two and four in each direction compared with the DNS were also computed but are not reported here. Both 5P-K1 and 5P-K2 are computed with LES.

Combustion is modeled by a premixed manifold approach (flamelet-generated manifolds; van Oijen & de Goey 2000). In this approach, solutions for one-dimensional premixed flat flames are precomputed, convoluted against a presumed subfilter PDF for the progress variable (beta distribution), and tabulated against the progress variable and its subfilter variance. During the LES calculations, transport equations are solved for the progress variable and its variance, and the thermochemical state is retrieved from the table of precomputed and preconvoluted one-dimensional premixed flat flames. The one-dimensional premixed flat flames are computed using FlameMaster (Pitsch 1998), and the chemical mechanism is the same as that used in the DNS. For 5P-K1, Lewis numbers are the same as those used in the DNS; for 5P-K2, the effective Lewis numbers are presumed to be unity owing to the influence of turbulent mixing (Savard & Blanquart 2014).

LES results with different subfilter transport models for the mean streamwise velocity are presented in Figure 3(a,b). For 5P-K2, all LES models predict roughly the same mean velocity profile, and the profiles rapidly converge to the DNS as the LES grid is refined.

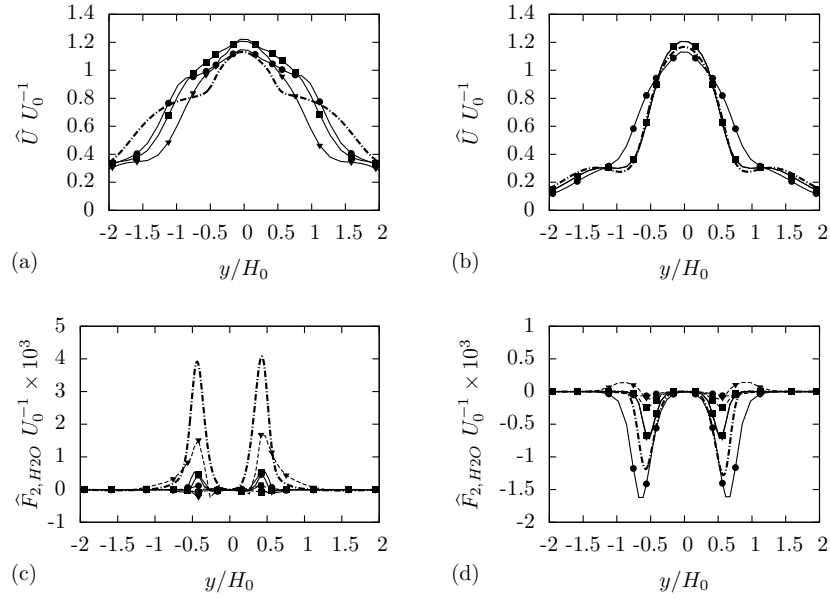


FIGURE 3. *A-posteriori* comparison of three LES subfilter transport models and DNS. The dot-dashed lines correspond to the DNS. For LES, the Smagorinsky(-like) model is labeled with squares (\blacksquare), the Clark model is labeled with circles (\bullet), and the linear algebraic heat-release model is labeled with triangles (\blacktriangledown). Top row: mean streamwise velocity; bottom row: mean cross-stream subfilter H_2O mass fraction flux. (a,c) 5P-K1, (b,d) 5P-K2. For (c,d), solid lines correspond to resolved contributions, and dashed lines correspond to subfilter contributions.

For 5P-K1, all the LES models predict visually different mean velocity profiles, and none match the DNS profile particularly well. As will be shown subsequently, this divergence in the predicted mean streamwise velocity profile is mirrored by poor predictions of turbulent transport combined with the extremely significant role of the flame in the generation of turbulence.

Figure 3(c,d) shows the mean cross-stream subfilter H_2O mass fraction flux. In the statistical sense, the cross-stream scalar flux is essentially aligned with the flame-normal vector. For 5P-K2, all models qualitatively agree with the DNS: the scalar flux is gradient. With all models, the resolved contribution to the scalar flux is significantly larger than that to the subfilter flux, even on this coarse grid, and the resolved contribution agrees in magnitude with the DNS, with the magnitude predicted by the Clark model being slightly larger than the magnitude of the DNS and the Smagorinsky-like and LAHR models being slightly smaller. The subfilter contributions to the scalar flux do qualitatively differ, with only the LAHR model predicting countergradient subfilter scalar flux, but the magnitude is small and inconsequential. The agreement in the mean streamwise velocity profiles in Figure 3(a,b) is attributed to this qualitative agreement in the turbulent mixing rate.

Conversely, Figure 3(c) shows significant qualitative differences in the scalar flux predictions for 5P-K1. The normalized scalar flux is countergradient and significantly larger in magnitude for 5P-K1 than for 5P-K2. All three models predict resolved scalar fluxes that are smaller than those of the DNS. The subfilter contribution from the Smagorinsky-like model is both small in magnitude and negative, that is, gradient transport, which

is qualitatively incorrect. While the Clark model does predict the correct sign of the subfilter contribution to the scalar flux (countergradient), the magnitude is far too small compared with that from the DNS data. These two trends in the subfilter fluxes are consistent with the *a priori* analysis shown in Figure 1, but the Clark model's underprediction of the scalar flux magnitude is more severe owing to the nonlinear dynamic feedback into the evolution of the resolved scales. For the LAHR model, the subfilter contribution to the scalar flux is significantly larger than that for the Clark model and closer but still smaller than that for the DNS, again consistent with the *a priori* analysis in Figure 1. Unlike the Clark model, the LAHR model directly uses information about the small-scale flame structure, so the influence of dynamic feedback is presumably less severe and partially explains the improved magnitude compared with that from the DNS. These significant differences in the turbulent mixing between the models and compared with the DNS are undoubtedly responsible for the poor predictions of the mean streamwise velocity profile.

4. Scaling arguments: validation and challenges

The scaling of the subfilter statistics with the filter width in the low- and high-Karlovitz-number regimes is now compared. In nonreacting turbulence, dimensional arguments based on Kolmogorov's hypotheses give the scaling of the progress variable dissipation rate, $\chi \equiv 2D\partial C/\partial x_j \partial C/\partial x_j$, where D is the mixture-averaged diffusivity, as $\chi \sim C_\Delta^2/t_\Delta \sim C_\Delta^2(\epsilon/\Delta^2)^{1/3}$, where C_Δ is the characteristic filter-scale fluctuation of the progress variable. Similarly, the TKE dissipation rate scales as $\epsilon \sim u_\Delta^3/\Delta$, where u_Δ is the characteristic filter-scale fluctuation of the velocity. The progress variable and filter-scale velocity therefore scale as $C_\Delta \sim (\chi/\epsilon)^{1/2}\Delta^{1/3}$ and $u_\Delta \sim \epsilon\Delta^{1/3}$, respectively. Since the majority of subfilter energy can be assumed to be contained in scales just smaller than the filter width, the Kolmogorov scaling for the subfilter scalar flux and the subfilter stress is $\widetilde{u''_j C''} \sim u_\Delta C_\Delta \sim (\chi\epsilon)^{1/2}\Delta^{2/3}$ and $\widetilde{u''_i u''_j} \sim u_\Delta u_\Delta \sim \epsilon^2\Delta^{2/3}$, respectively.

Figure 4(a,d) shows the scaling of the maximum $\hat{F}_{2,\text{H}_2\text{O}}$, both from DNS and *a priori* models, with the filter width. Figure 4(b,e) shows the L_2 error between the DNS-evaluated and *a priori*-modeled subfilter scalar flux (instantaneous spanwise mean), and Figure 4(c,f) shows the analogous L_2 error between the DNS-evaluated and *a priori*-modeled subfilter shear stress.

In both 5P-K1 and 5P-K2, the DNS-evaluated subfilter scalar flux scales as $\Delta^{5/3}$ rather than $\Delta^{2/3}$, but Kolmogorov scaling is not necessarily expected in reacting flows. Coincidentally, the subfilter scalar flux scales similarly in the two flames despite having opposite signs (see Figure 1). The Smagorinsky and Clark models generally match this scaling, but the Clark model always underpredicts the DNS statistics, with the difference becoming greater with increasing filter width in 5P-K2. The LAHR model overpredicts the DNS statistics at small filter widths, for which the flame structure is locally resolved and the thin flame assumption is invalid. Overall accuracy trends in the two flames are similar with two exceptions. First, the Smagorinsky model incorrectly captures the sign of $\hat{F}_{2,\text{H}_2\text{O}}$ in 5P-K1 [see Figure 1(a)] and is therefore much less accurate than the LAHR and Clark models. Second, only the Clark model captures the counter-Boussinesq transport of $\hat{\tau}_{12}^r$ in 5P-K1 (see Figure 2). However, the accuracy of the Clark model is reduced more quickly with increasing filter width than the accuracy of the physics-based models. The underlying phenomena that lead to departure from Kolmogorov scaling and reduced accuracy of physics-based models clearly merit further investigation. Finally, these analyses are con-

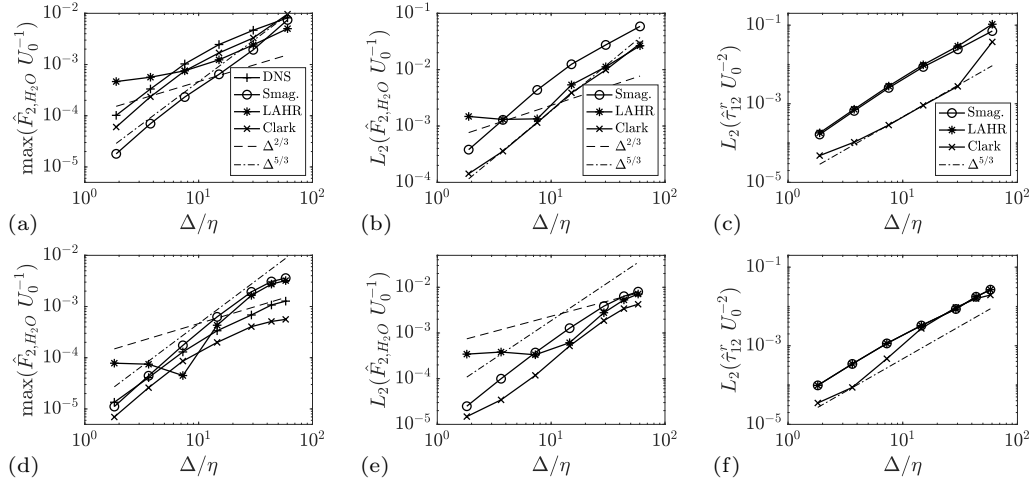


FIGURE 4. Scaling (a,d) and L_2 error (b,e) of the cross-stream subfilter scalar flux; L_2 error of the shear component of the subfilter stress (c,f) versus the filter width normalized by the Kolmogorov scale in the unburned gas. Top row: 5P-K1; bottom row: 5P-K2. For a description of lines in the bottom row, refer to legends in the top row.

cerned only with the low- and high-Karlovitz number regimes, and a potentially richer spectrum of interactions could occur in the intermediate regime of active-cascade energy transfer (moderate Karlovitz number and high Damköhler number). However, the scale separation necessary to parameterize over even one decade of Da_Δ at moderate Karlovitz number would necessitate extremely expensive calculations, pushing the limits of current computational capability. DNS and experimental databases in this intermediate regime are essential for future investigations of heat-release effects on subfilter turbulence as well as the development of advanced physics-based subfilter closures.

5. Conclusions

Three subfilter turbulence models have been evaluated in the low and high Karlovitz number regimes of turbulent premixed combustion. In a high-Karlovitz-number jet flame, Smagorinsky-like models are found to be accurate on average despite small amounts of local countergradient and counter-Boussinesq transport. The model of Clark *et al.* (1979) captures most local transport but underpredicts its magnitude, and the difference increases with increasing LES filter width. Conversely, in an analogous low-Karlovitz-number jet flame, Smagorinsky-like models predict the opposite direction of transport, which can be corrected by linear algebraic closures in the infinitely thin flame limit when the countergradient transport occurs on average in the flame-normal direction. When applied to LES calculations, the linear algebraic closure for the scalar flux predicts the greatest subfilter contribution of the three models due to the additional modeled subfilter physics. However, more complex closures for the subfilter stress are necessary, and further research on the departure from Kolmogorov scaling in the low- and high-Karlovitz-number regimes could inform the development of such closures. Finally, research on the intermediate, active-cascade regime is desperately needed and will require DNS and/or experimental databases at moderate Karlovitz number and high Damköhler number.

Acknowledgments

The authors are grateful for helpful discussions with Dr. Javier Urzay, Dr. Timothy Gallagher, and Dr. Ayaboe Edoh. Computational support was provided by the TIGRESS High-Performance Computer Center at Princeton University and the National Energy Research Scientific Computing Center (NERSC).

REFERENCES

- BILGER, R. W. 2004 Some aspects of scalar dissipation. *Flow, Turbul. Combust.* **72**, 93–114.
- BRAY, K. N. C., LIBBY, P. A., MASUYA, G. & MOSS, J. B. 1981 Turbulence production in premixed turbulent flames. *Combust. Sci. Technol.* **25**, 127–140.
- CHENG, R. K. 1984 Conditional sampling of turbulence intensities and Reynolds stress in premixed turbulent flames. *Combust. Sci. Technol.* **41**, 109–142.
- CLARK, R. A., FERZIGER, J. H. & REYNOLDS, W. C. 1979 Evaluation of subgrid-scale models using a fully simulated turbulent flow. *J. Fluid Mech.* **91**, 1–16.
- HAMLINGTON, P. E., POLUDNENKO, A. Y. & ORAN, E. S. 2011 Interactions between turbulence and flames in premixed reacting flows. *Phys. Fluids* **23**, 125111.
- MACART, J. F., GRENGA, T. & MUELLER, M. E. 2018 Effects of combustion heat release on velocity and scalar statistics in turbulent premixed jet flames at low and high Karlovitz numbers. *Combust. Flame* **191**, 468–485.
- MOSS, J. B. 1980 Simultaneous measurements of concentration and velocity in an open premixed turbulent flame. *Combust. Sci. Technol.* **22**, 119–129.
- O'BRIEN, J., TOWERY, C. A. Z., HAMLINGTON, P. E., IHME, M., POLUDNENKO, A. Y. & URZAY, J. 2017 The cross-scale physical-space transfer of kinetic energy in turbulent premixed flames. *Proc. Combust. Inst.* **36**, 1967–1975.
- O'BRIEN, J., URZAY, J., POLUDNENKO, A. Y., HAMLINGTON, P. E. & IHME, M. 2014 Counter-gradient subgrid-scale transport and energy backscatter in turbulent deflagrations. *Proceedings of the Summer Program*, Center for Turbulence Research, Stanford University, pp. 147–157.
- VAN OIJEN, J. A. & DE GOEY, L. P. H. 2000 Modelling of premixed laminar flames using flamelet-generated manifolds. *Combust. Sci. Technol.* **161**, 113–137.
- PITSCH, H. 1998 FlameMaster, A C++ computer program for 0D combustion and 1D laminar flame calculations.
<https://web.stanford.edu/group/pitsch/FlameMaster.htm>.
- SAVARD, B. & BLANQUART, G. 2014 An a priori model for the effective species Lewis numbers in premixed turbulent flames. *Combust. Flame* **161**, 1547–1557.
- TOWERY, C. A. Z., POLUDNENKO, A. Y., URZAY, J., O'BRIEN, J., IHME, M. & HAMLINGTON, P. E. 2016 Spectral kinetic energy transfer in turbulent premixed reacting flows. *Phys. Rev. E* **93**, 053115.
- VEYNANTE, D., TROUVÉ, A., BRAY, K. N. C. & MANTEL, T. 1997 Gradient and counter-gradient scalar transport in turbulent premixed flames. *J. Fluid Mech.* **332**, 263–293.